Science Signaling
AAAS

The Specificity of Innate Immune Responses Is Enforced by Repression of Interferon Response Elements by NF-{kappa}B p50

Christine S. Cheng, Kristyn E. Feldman, James Lee, Shilpi Verma, De-Bin Huang, Kim Huynh, Mikyoung Chang, Julia V. Ponomarenko, Shao-Cong Sun, Chris A. Benedict, Gourisankar Ghosh and Alexander Hoffmann (22 February 2011)
Science Signaling **4** (161), ra11. [DOI: 10.1126/scisignal.2001501]

Science Signaling (ISSN 1937-9145) is published weekly, except the last week in December, by the American Association for the Advancement of Science, 1200 New York Avenue, NW, Washington, DC 20005.

GENE EXPRESSION

The Specificity of Innate Immune Responses Is Enforced by Repression of Interferon Response Elements by NF-κB p50

Christine S. Cheng,[1,2,3] Kristyn E. Feldman,[1,2] James Lee,[1,2] Shilpi Verma,[4] De-Bin Huang,[2] Kim Huynh,[2] Mikyoung Chang,[5] Julia V. Ponomarenko,[6] Shao-Cong Sun,[5] Chris A. Benedict,[4] Gourisankar Ghosh,[2] Alexander Hoffmann[1,2,3]*

The specific binding of transcription factors to cognate sequence elements is thought to be critical for the generation of specific gene expression programs. Members of the nuclear factor κB (NF-κB) and interferon (IFN) regulatory factor (IRF) transcription factor families bind to the κB site and the IFN response element (IRE), respectively, of target genes, and they are activated in macrophages after exposure to pathogens. However, how these factors produce pathogen-specific inflammatory and immune responses remains poorly understood. Combining top-down and bottom-up systems biology approaches, we have identified the NF-κB p50 homodimer as a regulator of IRF responses. Unbiased genome-wide expression and biochemical and structural analyses revealed that the p50 homodimer repressed a subset of IFN-inducible genes through a previously uncharacterized subclass of guanine-rich IRE (G-IRE) sequences. Mathematical modeling predicted that the p50 homodimer might enforce the stimulus specificity of composite promoters. Indeed, the production of the antiviral regulator IFN-β was rendered stimulus-specific by the binding of the p50 homodimer to the G-IRE–containing *IFN*β enhancer to suppress cytotoxic IFN signaling. Specifically, a deficiency in p50 resulted in the inappropriate production of IFN-β in response to bacterial DNA sensed by Toll-like receptor 9. This role for the NF-κB p50 homodimer in enforcing the specificity of the cellular response to pathogens by binding to a subset of IRE sequences alters our understanding of how the NF-κB and IRF signaling systems cooperate to regulate antimicrobial immunity.

INTRODUCTION

The cellular innate immune response is triggered by three families of extracellular and intracellular receptors, which bind to a broad range of molecular patterns (*1*). The Toll-like receptors (TLRs), the retinoic acid–inducible gene 1 (RIG-1)–like receptors (RLRs), and the nucleotide-binding oligomerization domain (NOD)–containing protein–like receptors (NLRs) show specificity in their recognition of pathogen-associated molecular patterns (PAMPs) and metabolic products, which are termed danger-associated molecular patterns (DAMPs). Although many cell types are capable of mounting innate immune responses, macrophages are professional, tissue-resident initiators, coordinators, and effectors of the innate immune response.

Pathogen recognition by macrophages elicits gene expression programs that typically consist of hundreds of genes (*2*–*4*), which may be broadly classified as mediating cellular antiviral functions and systemic immune activation through inflammation (*5*). Because both types of responses are also potentially detrimental to the organism (*6*–*8*), cells are thought to produce pathogen-specific responses, ensuring that unnecessary gene products are not made. Dozens of transcription factors have been implicated in enabling the fine-tuned expression of genes whose products mediate the innate immune response (*9*, *10*); however, the identities of the critical regulators of pathogen- or stimulus-specific gene expression remain an open question that is of relevance to an understanding of antimicrobial immune responses, chronic inflammatory disease, and the development of relevant therapeutics, including adjuvants for innate and adaptive immune responses.

Two families of transcriptional regulators that play central roles in coordinating the gene expression programs of the cellular innate immune response are the nuclear factor κB (NF-κB) and interferon (IFN) regulatory factor (IRF) families (*3*, *11*–*15*) (Fig. 1A). Stimulus-dependent activation of NF-κB and IRFs is determined by signaling adaptors that selectively interact with the intracellular domains of TLRs (*16*). Myeloid differentiation marker 88 (MyD88) mediates the activation of NF-κB and is associated with most TLRs, including TLR9, which senses bacterial CpG-rich DNA, and TLR4, the sensor for the Gram-negative bacterial cell wall component lipopolysaccharide (LPS). Toll–interleukin-1 (IL-1) receptor (TIR) domain–containing adaptor-inducing IFN-β (TRIF) functions as the primary signaling adaptor for the activation of IRFs and is associated with some TLRs, including TLR4, but not TLR9. Hence, each TLR produces a characteristic combination of transcription factor activities, including those of NF-κB and the IRFs.

NF-κB and the IRFs constitute families of transcription factors that are defined by conserved DNA binding domains. In macrophages, IRF3 is activated through its site-specific phosphorylation by TANK-binding kinase 1 (TBK1) (*17*), an important effector kinase of the TRIF pathway. IRF3-driven production of type I IFN results in an autocrine loop that activates a second IRF family member, IFN-α–stimulated gene factor 3 (ISGF3), whose DNA binding component is IRF9. IRF3 and ISGF3 appear to have largely overlapping DNA binding specificities for the IFN

[1]Signaling Systems Laboratory, University of California–San Diego, 9500 Gilman Drive, La Jolla, CA 92093, USA. [2]Department of Chemistry and Biochemistry, University of California–San Diego, La Jolla, CA 92093, USA. [3]San Diego Center for Systems Biology, University of California–San Diego, La Jolla, CA 92093, USA. [4]Division of Immune Regulation, La Jolla Institute for Allergy and Immunology, La Jolla, CA 92037, USA. [5]Department of Immunology, University of Texas MD Anderson Cancer Center, 7455 Fannin Street, Houston, TX 77030, USA. [6]San Diego Supercomputer Center, University of California–San Diego, La Jolla, CA 92093, USA.
*To whom correspondence should be addressed. E-mail: ahoffmann@ucsd.edu

response element (IRE) consensus sequence (AANNGAAA) (*18*). Within the NF-κB family, the key transcriptional effectors are the activation domain–bearing RelA and cRel proteins, which as dimers with the *nfkb1* gene product p50 are responsible for κB-driven gene activation. Overlapping DNA binding specificities for the broad κB consensus sequence [GGRNNN(N)YCC] (*19*) underlie the fact that there have only been isolated reports of specific cRel or RelA target genes (*20*, *21*).

However, another major NF-κB family member is the p50 homodimer (p50-p50), a presumptive transcriptional repressor of κB sites by virtue of its close sequence and structural homology with other NF-κB family members and its lack of a transcriptional activation domain (*22*, *23*). Indeed, p50-p50 acts as a competitive repressor of κB-driven transcription in transiently transfected cells and in studies performed in vitro (*24*, *25*) and may repress the expression of the *tumor necrosis factor* (*tnf*) gene (*26*–*28*);

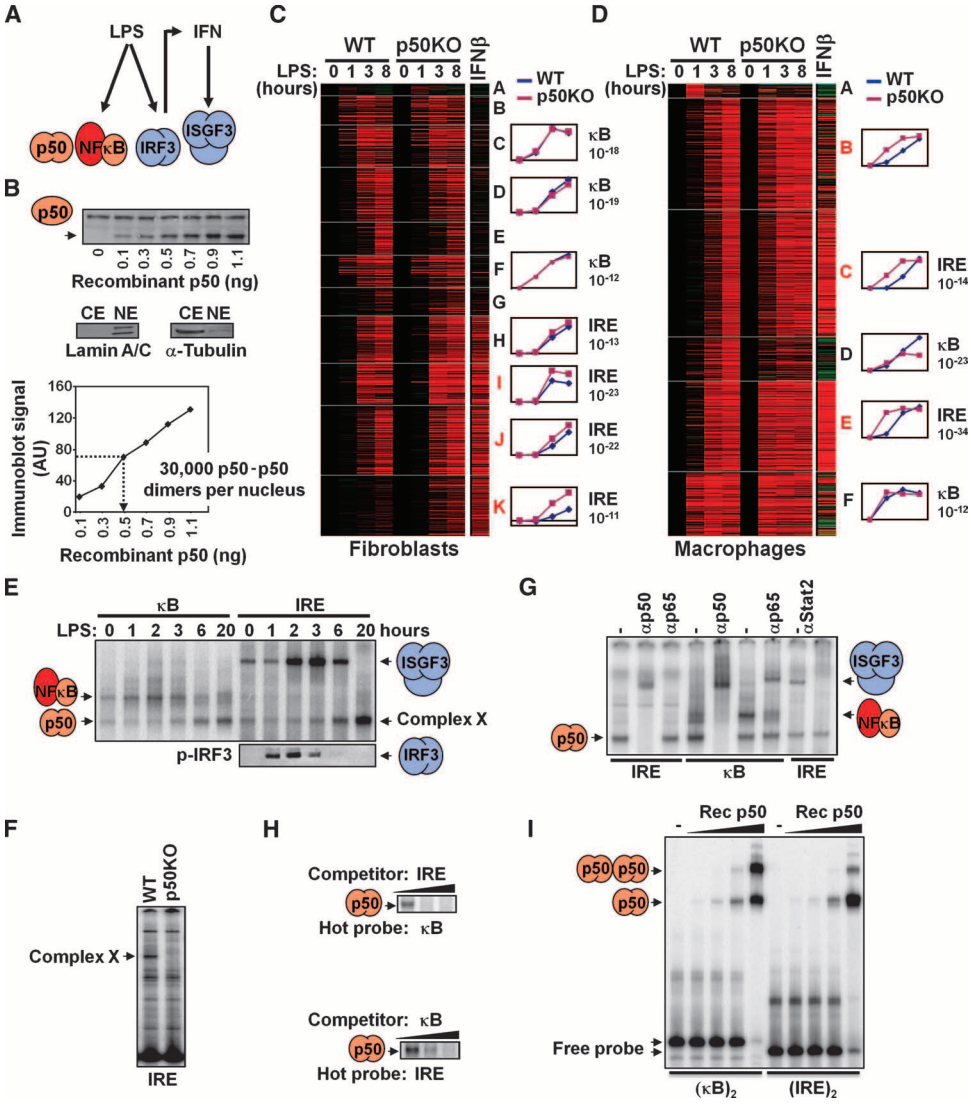

Fig. 1. NF-κB p50 represses IFN response genes and may physically bind to IRE sequences. (**A**) A schematic of LPS- and IFN-β–induced activation of NF-κB, IRF3, and ISGF3 and of p50-p50. (**B**) Quantitation of the basal amounts of nuclear p50 protein by Western blotting analysis of a nuclear extract prepared from untreated wild-type (WT) BMDMs mixed with increasing amounts (0.1 to 1.1 ng) of recombinant p50 (amino acid residues 1 to 325). Nuclear and cytoplasmic fractionation was confirmed by Western blotting analysis for lamin A/C and α-tubulin (lower panel). The amounts of p50 were quantitated and graphed on a standard curve, leading to an estimate of 30,000 p50 homodimers per nucleus. (**C** and **D**) Microarray mRNA expression data from WT and *nfkb1*$^{-/-}$ ("p50KO") littermate-derived MEFs stimulated with LPS (0.1 μg/ml) and IFN-β (2500 U/ml) (C) or from BMDMs stimulated with LPS (0.1 μg/ml) and IFN-β (10 U/ml) (D) were analyzed by *K*-means clustering. Red represents stimulus-responsive gene induction, whereas green represents repression. Cluster identifiers are indicated on the right, with red symbols indicating clusters with increased expression in the p50KO cells compared to that in WT cells. The average fold induction (log_2) of each cluster in WT (blue) and p50KO (purple) cells was graphed at 0, 1, 3, and 8 hours. The most highly enriched motifs identified de novo within −1.0 to +0.3 kb of the transcriptional start sites are shown in each cluster, with *P* values to indicate statistical significance. (**E**) Transcription factor activation in RAW264.7 cells in response to LPS (0.1 μg/ml). κB-binding activities (p50-p65 and p50-p50, left panel) and IRE-binding activities (ISGF3 and complex X, right panel) on an IRE probe (GATCCTCGGGAAAGGGAAACCTAAACTGAAGCC) were revealed by EMSA. Western blotting analysis (bottom right) shows the activation profile for nuclear phosphorylated IRF3 (p-IRF3 at Ser^{396}). (**F**) IRE-binding activities contained in nuclear extracts derived from WT and p50KO BMDMs stimulated with LPS (0.1 μg/ml) for 24 hours were resolved by EMSA. (**G**) The composition of the complex was examined by supershift analysis with the indicated antibodies (indicated by α) on the IRE probe and by comparison to the mobilities of complexes bound to an HIV κB site probe. (**H**) DNA binding site competition assays (10- or 200-fold excess) with labeled κB probe and unlabeled IRE probe (top panel), or with labeled IRE probe and unlabeled κB probe (bottom panel) and nuclear extracts from RAW264.7 cells stimulated with LPS for 24 hours. (**I**) Measurement by EMSA of the relative binding affinities of p50-p50 for κB or IRE probes. Increasing amounts of recombinant p50 (1, 10, 100, and 1000 ng) were incubated with a κB site probe containing two κB-binding sites (left panel) or an IRE probe containing four IRE-binding sites (right panel). Both probes enable the binding of two p50 dimers. Data are from, or representative of, at least three experiments.

however, the binding specificity and physiological functions of this putative transcriptional repressor remain uncharacterized. Whereas the role of p50 as a dimerization partner for RelA and cRel is compensated for by the *nfkb2* gene product p52 (*21*), p50-p50 may play unique functions as a repressor within the NF-κB family. Within the innate immune response, during which inappropriate gene expression is potentially detrimental for cellular or organismal health, the role of transcriptional repressors is of pertinent interest. To characterize the physiological role of p50-p50 in the innate immune response, we first undertook unbiased genome-wide studies to identify its functional targets and then characterized the molecular mechanism of p50-p50 at the level of biophysical DNA binding specificity and within the context of the gene regulatory circuitry of composite enhancer elements.

RESULTS

NF-κB p50 represses IFN response genes

To characterize the functional role of p50-p50 in the immune response in macrophages, we first determined its abundance by quantitative Western blotting analysis. Through the use of recombinant protein standards, we estimated that there were 30,000 p50 homodimers in the nuclei (equivalent to a concentration of 200 nM) in naïve or resting bone marrow–derived macrophages (BMDMs) (Fig. 1B). To identify functional targets of p50-p50 during the cellular response to pathogens in an unbiased manner, we profiled gene expression induced by LPS in $nfkb1^{-/-}$ [p50 knockout (p50KO)] cells by microarray analysis. We used *K*-means clustering to analyze relevant microarray data sets generated with murine embryonic fibroblasts (MEFs), and we used bioinformatics to identify shared sequences in the promoters of coregulated genes (Fig. 1C). We found that p50KO cells exhibited the enhanced expression of genes that are not known to be regulated by NF-κB (Fig. 1C, clusters I to K). We found that these genes were inducible by IFN and contained IREs in their promoter sequences. Similar studies with BMDMs also revealed a p50-mediated repressive effect on sets of IRE-containing genes in response to LPS (Fig. 1D, clusters B, C, and E) or in response to moderate stimulation with IFN-β (fig. S1, clusters B and C). The known function of p50 as a binding partner for the transcriptional activator RelA was apparent in only a small reduction in the extent of expression of some NF-κB–regulated genes (Fig. 1C, clusters C and D, and Fig. 1D, clusters D and F), indicating redundancy with p52 or the presence of RelA homodimers, or that the repressive functions of p50-p50 masked the stimulatory effects of p50:RelA (*21*).

The *nfkb1* gene gives rise to two gene products through a protein-processing mechanism, the mature p50 protein and its precursor form, p105, which may sequester activating NF-κB subunits (*29*) and participate in extracellular signal–regulated kinase (ERK) signaling (*30*, *31*). When we examined LPS-induced gene expression profiles in BMDMs from wild-type and $p105^{-/-}$ mice, which lack p105 but produce p50 (*32*), we did not observe an increase in the expression of IFN-inducible genes in the $p105^{-/-}$ cells (fig. S2). Our results suggest that the mature p50 protein participates in the regulation of IFN response genes, either directly or indirectly. To characterize the proteins that bound to IRE targets, we performed electrophoretic mobility shift assays (EMSAs) with a widely used IRE probe (*33*). Time course studies confirmed that LPS activated the transcriptional activators NF-κB (the p65-p50 heterodimer), IRF3, and subsequently ISGF3 [IRF9 associated with signal transducer and activator of transcription 1 (STAT1) and STAT2], whereas the κB-binding activity of the transcriptional repressor p50-p50 was constitutive in resting cells and was increased at late time points (Fig. 1E and fig. S3) because of NF-κB (p65-p50)–induced transcriptional activation of *nfkb1* (*34*). We observed the formation of an unexpected complex ("complex X") on the IRE probe (Fig. 1E). Not only did this complex have the same mobility as that of p50-p50 on the κB probe, but it was also absent from p50-deficient BMDMs (Fig. 1F). Antibody supershifts showed that this complex contained p50 but not p65 (Fig. 1G). Competition assays with cold probe showed that the IRE and κB probes cross-competed for binding to p50-p50 (Fig. 1H), and titration of recombinant p50 protein on IRE and κB probes indicated that p50-p50 had similar affinities for the sequences in IRE and κB sites (Fig. 1I). Together, our results suggest that the constitutively present p50 homodimer may repress IFN-inducible genes by binding directly to IRE sites.

NF-κB p50 binds to and regulates "G-IREs"

When we examined the promoter sequences of well-known IRF target genes, we found that genes that showed enhanced expression in p50KO compared to wild-type cells tended to contain guanine-rich (G-rich) sequences within or next to their IREs (Fig. 2A, red), whereas other genes that showed little change in expression in p50KO cells did not (Fig. 2A, black). To evaluate the role of the G-rich sequence statistically, we generated replicate microarray data sets from LPS-treated BMDMs. We focused on IFN-inducible genes whose activation by LPS was dependent on the type I IFN receptor [IFN-α receptor (IFNAR)] and we found a continuum of enhanced expression phenotypes in LPS-induced p50KO cells (Fig. 2B), consistent with a range of relatively different numbers of binding sites or DNA binding affinities of p50 and IRF. By labeling those genes whose regulatory regions contained G-rich IREs as "G-IREs," we observed that G-IREs were overrepresented in genes whose expression in response to LPS was enhanced in p50KO cells compared to that in wild-type cells (Fig. 2B). Exceptions to this correlation were also apparent and may have been a result of transcriptional saturation effects, dysregulation of the ERK pathway (*30*, *31*) or the production of IFN, or the likely possibility that the G-rich classification may have in some cases considered IRE-like sequences that are not functionally relevant. However, statistical evaluation indicated that G-IRE–containing IFN-inducible genes were more likely than their non–G-rich counterparts to be dysregulated in p50KO cells (Fig. 2C, $P < 0.0001$). Furthermore, endogenous p50-p50 formed complexes with DNA probes that contained the IRE-containing regulatory sequences derived from several p50-repressed genes, but not when the DNA probes contained analogous sequences from p50-independent genes (Fig. 2D). Chromatin immunoprecipitation (ChIP) assays revealed recruitment of p50 to those endogenous IRF target genes that showed enhanced expression in p50-deficient cells compared to that in wild-type cells, but less recruitment of p50 to those IRF target genes that were largely independent of p50 (Fig. 2E). Control experiments confirmed that NF-κB p65 was not recruited to either class of IRF target genes (Fig. 2F), whereas ISGF3 was recruited to both classes of genes (fig. S4).

On the basis of the crystal structures of NF-κB bound to near-palindromic κB sites (*35*, *36*), we modeled p50-p50 bound to the G-IRE and IRE sequences of *Gbp1* (Fig. 3A). We hypothesized that the first p50 monomer was likely to make base-specific contacts with the G-IRE sequence, which conforms to the first half of the palindromic κB consensus site (5′-GGRN-3′) (Fig. 3B), whereas the second p50 monomer would not make base-specific contacts with the second IRE because it deviates substantially from the second half of the κB consensus sequence (Fig. 3C). However, the central tyrosine clamp of both monomers might contribute to the stability of the complex because it is largely sequence-independent. We reasoned that the hinge region between the DNA binding and the dimerization domains within the Rel homology region of the second p50 monomer would assume different angles from those of the first monomer. Such structural considerations suggest that a single half-site containing three or four

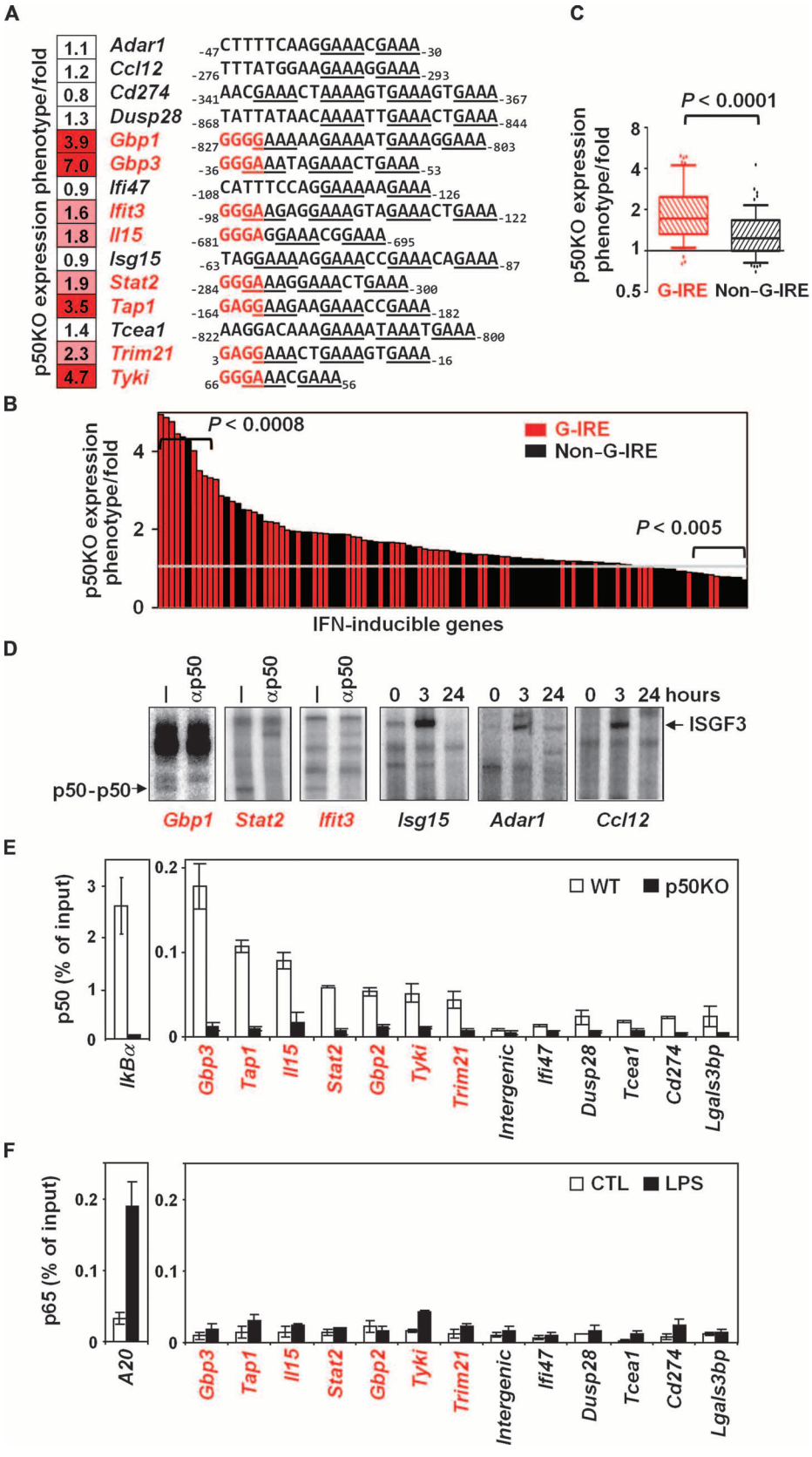

Fig. 2. NF-κB p50 binds to a subset of IFN response genes through a G-IRE sequence. (**A**) Known IRE-regulated genes are categorized into those that are repressed (red) or not repressed (black) by p50. IRE sequences are underlined, and G-rich sequences are highlighted in red. The p50KO expression phenotype represents the ratio of the LPS-induced (0.1 μg/ml for 6 hours) fold change in expression of genes in p50KO compared to that of WT BMDMs in duplicate microarray experiments. Fold changes <1.5 are in white boxes; fold changes ≥1.5 and <3 are in pink; fold changes ≥3 are in red. (**B**) p50KO expression phenotype (*y* axis) for 107 IFN-β–inducible and IFNAR-dependent, LPS-inducible genes (*x* axis). Genes that contain one or more G-IREs in the regulatory region located from −1.0 to +0.5 kb of the transcription start site are colored red. Probabilities that the numbers of G-IRE–containing genes that were among the top or bottom 10% of genes within distribution occurred by chance are indicated. (**C**) Unpaired *t* test of the p50KO expression phenotype associated with G-IRE (red)– and non–G-IRE (black)–containing genes in (B). Edges of the box plot represent the 25th and 75th percentiles, and whiskers represent the 10th and 90th percentiles. (**D**) The DNA binding activities of p50-p50 and ISGF3 were resolved by EMSA and supershift assays with antibody against p50 with extracts of RAW264.7 cells stimulated with LPS (0.1 μg/ml) for 24 hours with probes derived from p50-repressed genes that contain G-IREs (red) or probes derived from p50-independent genes that contain non–G-IREs (black). (**E**) ChIP followed by qPCR analysis indicated the recruitment of p50 to the p50-repressed (and G-rich, in red) but not to p50-independent (and non–G-rich, in black) IRE sequences in WT (white bar) and p50KO (black bar) BMDMs stimulated with LPS (0.1 μg/ml) for 24 hours. IκBα (inhibitor of NF-κBα) was a positive control for NF-κB target genes. (**F**) ChIP and qPCR analysis of the recruitment of p65 to p50-repressed G-IREs (red) and p50-independent non–G-rich IREs (black), as well as the positive control κB target gene (*A20*) in response to LPS (0.1 μg/ml, black bar) or phosphate-buffered saline (PBS) [control (CTL), white bar] for 1 hour in WT BMDMs. Data are from, or representative of, at least three experiments.

guanines would provide a sufficient number of contacts with the first p50 monomer to enable high-affinity binding (Fig. 3B), whereas the second monomer may accommodate suboptimal sequences by avoiding disallowed contacts (Fig. 3C) as a result of rotational flexibility (about 18°) between its DNA binding and dimerization domains (Fig. 3A). Indeed, mutation of the binding site confirmed that the G's within the first IRE was critical for the binding of purified recombinant p50-p50, whereas the analogous positions within the second IRE were not (Fig. 3D). Thus, our analysis suggests a model of p50-p50-IRE binding in which the interaction of one monomer with a G-IRE provides sufficient affinity, whereas the second monomer has rotational flexibility to accommodate a nonconsensus sequence.

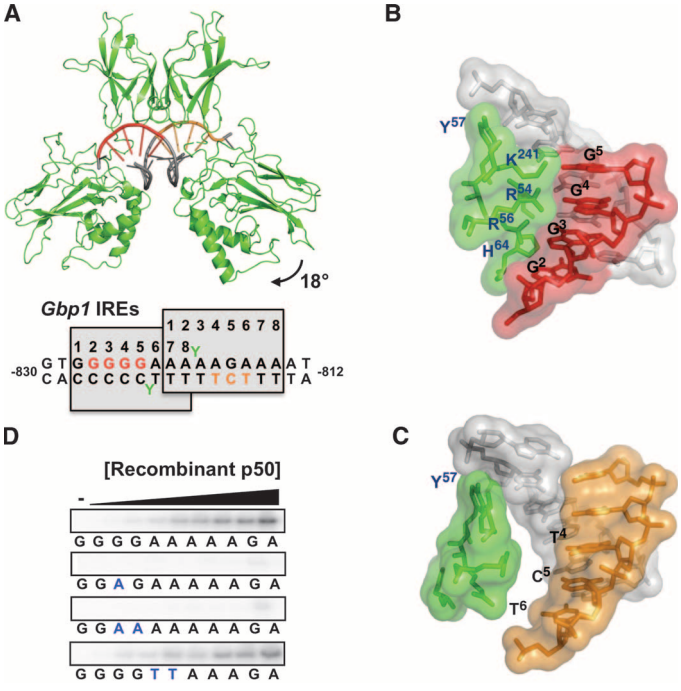

Fig. 3. Molecular determinants of the binding of p50-p50 to a G-IRE sequence. (**A**) Ribbon model of the structure of p50-p50 on the G-IRE and IRE of *Gbp1*, based on previous x-ray crystallography structures of p65-p50 on κB sites (*36*). In both the ribbon model and the G-IRE sequence, the DNA in the vicinity of the first monomer is indicated in red, whereas the DNA in the vicinity of the second monomer is in orange. Conserved tyrosine residues (Y) that contribute to the stability of the complex by inserting themselves between bases are indicated in green. Rotational flexibility between the DNA and the dimerization domains of the second monomer is indicated. (**B**) Space-filling model detailing the amino acid residues within the first monomer that make close contacts with the G-IRE sequence. Numbering is with respect to the center of a palindromic sequence that would apply to the κB consensus sequence. (**C**) Space-filling model revealing a gap between the protein surface and the second IRE sequence within *Gbp1*. This gap is opened by the rotational flexibility between the dimerization and the DNA binding domains. Note that Tyr^{57} stabilizes the complex because it is anchored by hydrogen bonds to the phosphate backbone and makes van der Waals contacts with the bases A2 and A3 of the second IRE. (**D**) Determination of the binding specificity of p50-p50 for IREs by EMSA by titrating recombinant p50 proteins (1, 5, 10, 20, 40, 80, 200, and 500 nM) with the G-IRE–containing probe derived from Gbp1 or indicated mutant variants thereof. Data are from, or representative of, at least three experiments.

Functional consequences of interactions between p50-p50 and G-IREs

Next, we studied the immediate functional consequences of the binding of p50-p50 to G-IRE sites. IRE-ISGF3 and IRE-IRF3 complexes formed in in vitro binding assays were competed for when we titrated the amount of recombinant p50 protein (Fig. 4A). We did not see this competitive effect when we titrated p65 protein or when we used DNAs that lacked G-rich sequences (Fig. 4B), and we never observed any higher-order complexes that contained both p50 and IRF proteins. Transient transfection studies revealed that only the expression of a form of p50 that was competent for DNA binding specifically reduced the IRF-mediated activation of a G-IRE–driven reporter gene (Fig. 4C), but not that of a non–G-IRE reporter gene (fig. S5). Our results suggest that p50-p50 may inhibit promoter activity by simply competing with IRF3 and ISGF3 for binding to G-IREs, although we cannot rule out the existence of an active repression mechanism that operates through the recruitment of corepressors.

To explore the functional consequences of the competition model for promoter activity, we used a thermodynamic model (*37*) to calculate fractional promoter activity as a function of the concentrations of p50-p50 and IRF (Fig. 4D). The model recapitulated our experimental finding that p50-repressed, G-IRE–containing genes were enhanced in expression in p50KO cells compared to that in wild-type cells, with the relative effect being more substantial at low concentrations of IRF (Fig. 4E), because they may occur in the early phases of a time course. Indeed, a simple parameter sensitivity analysis confirmed that the enhanced expression of genes in p50KO cells was not only a function of the affinity of p50-p50 for the IRE but was also more pronounced at low concentrations of IRF (Fig. 4F). G-IRE–containing promoters were more likely than non–G-IRE–containing promoters to show increased expression in unstimulated conditions in p50KO cells (figs. S2 and S6), presumably because of low, but functionally relevant, basal IRF3 activity.

The mathematical modeling approach lends itself to exploring the functional consequences of the regulation of G-IREs by p50-p50 on physiologically relevant gene regulatory circuits. Many genes involved in the innate immune response contain clusters of IRE and κB sites that are thought to function cooperatively to enable stimulus-specific control of gene expression (*38*–*40*). Such functional cooperativity may be described with a thermodynamic model for so-called AND-gate promoters (*37*, *41*). We derived an expression for the promoter activity of a gene whose duplicate IREs and a κB site synergized through cooperative IRF and NF-κB interactions and for which only the κB site was subject to repression by p50-p50 (Fig. 5A). As expected, the formulation showed that both NF-κB and IRF needed to be activated to induce the promoter; however, the promoter activity heat map showed that even low amounts of IRF activity were sufficient to render the promoter responsive to activation by NF-κB. PAMPs may be categorized into those that activate both NF-κB and IRF and those that activate NF-κB alone (*13*, *14*). For example, macrophages exposed to bacteria-derived, CpG-containing DNA activate NF-κB, whereas those cells exposed to LPS activate both NF-κB and IRF factors. Thus, basal activity of IRF3 (fig. S7) may result in the inappropriate induction of a promoter in response to stimuli, such as CpG, that only activate NF-κB. The modeling illustrates that AND-gates may be rendered surprisingly leaky when inducible transcription factors have substantial basal activity.

We constructed alternate thermodynamic models to explore the functional consequence of the repression of a G-IRE by p50-p50 within this AND-gate promoter architecture (Fig. 5B). The analogous promoter activity heat map showed that the expression of CpG-responsive genes was effectively abolished, but that responsiveness to LPS was preserved. The result was a sharpened stimulus specificity of the promoter, suggesting that p50-p50 may have gatekeeping functions on G-IRE–containing composite promoters. We examined whether this conclusion was dependent on

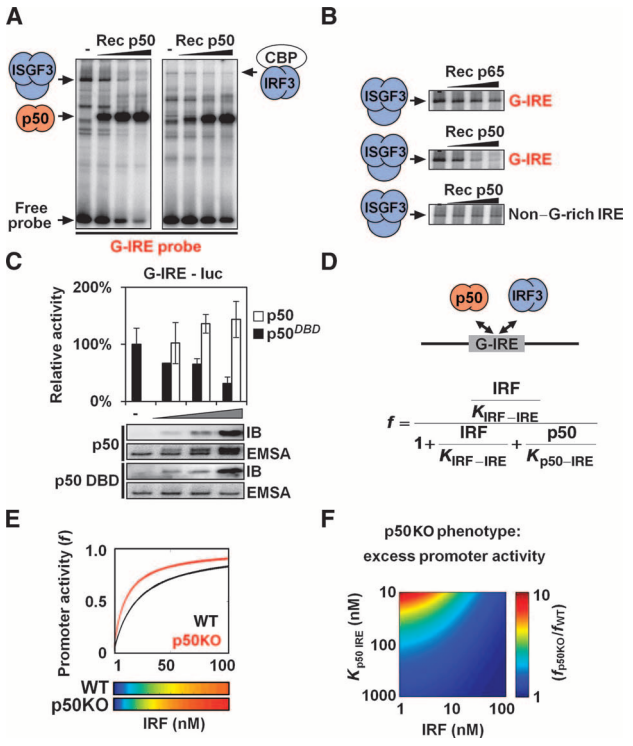

Fig. 4. p50-p50 represses G-IREs by competing with IRFs. (**A**) Competition EMSAs demonstrating that increasing amounts of recombinant p50-p50 (25, 250, and 1000 nM) compete with nuclear ISGF3 complexes [contained in LPS-stimulated (0.1 μg/ml, for 24 hours) RAW264.7 cells] for binding to the G-IRE probe (left) or with nuclear IRF3-CBP complexes [contained in polyI:C (polyinosine-polycytosine)–stimulated (5.0 μg/ml for 1 hour) HeLa cells] in binding to the *Gbp3* IRE probe (right). (**B**) Competition EMSAs demonstrating that nuclear ISGF3 complexes that bind to IRE probes were not efficiently competed for by recombinant p65-p65 (25, 250, and 1000 nM; upper panel), but were competed for by recombinant p50-p50 (25, 250, and 1000 nM, middle panel), and that ISGF3 complexes binding to the non–G-rich *ADAR1* IRE probe were not competed for by recombinant p50-p50 (25, 250, and 1000 nM; bottom panel). (**C**) p50, but not a p50 DBD mutant (R56A,Y57A), inhibited LPS-induced activation of G-IRE–containing promoters in a dose-dependent manner. TLR4–HEK 293T cells were transfected with IRE reporter plasmids (40 ng) and plasmids encoding p50 or the p50 DBD mutant (0, 40, 120, or 300 ng) in 24-well plates. Forty-eight hours later, cells were stimulated with LPS (0.1 μg/ml) for 6 hours. The relative luciferase activities of G-IRE– and non–G-rich IRE–containing reporters were graphed as a function of promoter activity in the absence of p50. Lower panel: Western blotting analysis of nuclear p50 protein and the IRE-binding activity of p50-p50 was resolved by EMSA (the lower band represents constitutively expressed endogenous p50-p50). (**D**) A schematic and thermodynamic formulation of promoter activity *f* (*37*) of a G-IRE–containing promoter subject to competitive binding by p50-p50 and IRFs. (**E**) The mathematical solution of promoter activity (*f*) in WT and p50KO cells as a function of the concentration of IRF. The colored bars represent promoter activity (*f*) in WT and p50KO cells, ranging from 0 (blue) to 1 (red). (**F**) Computational determination of the p50KO phenotype defined as the fold change in the activity (*f*) of a G-IRE–driven promoter between p50KO and WT cells as a function of the IRF concentration and the p50 dissociation constant for the IRE ($K_{p50\text{-}IRE}$). Data are from, or representative of, at least three experiments.

specific parameter values within these models of hypothetical response genes. A multidimensional parameter sensitivity analysis of the four relevant dissociation constants indicated that specificity for LPS rather than CpG was enhanced by the repression of the G-IRE by p50-p50 under various conditions and was never diminished. Such promoter "gating" to restrict gene expression to specific stimuli was independent of the binding of p50-p50 to the κB site (see low $K_{p50\text{-}IRE}$) and was strongest on promoters on which IRFs had moderate affinity but p50-p50 had stronger binding affinity (Fig. 5C). We note that G-IREs had high affinity for p50-p50 (Fig. 1) but may have suboptimal affinity for IRFs.

p50-p50 restricts antiviral responses to specific stimuli

To test the prediction that p50-p50 may enforce the stimulus specificity of AND-gate promoters, we examined one of the most well-studied and physiologically important composite promoters—that controlling the expression of IFN-β. Synergy between NF-κB and IRF transcription factors through coordinated DNA binding sites [so-called positive regulatory domain (PRD) elements] is critical for control of the expression of *IFN*β (*42*, *43*). p50 binds to the *IFN*β enhancer in unstimulated cells (*44*), but the ChIP assay is not of sufficient resolution to determine the precise location(s) of p50. Within the regulatory sequence, not only the κB site in PRDII but also the IREs in the PRDI and PRDIII regions contain G-rich sequences (Fig. 6A). Indeed, a DNA binding probe that encompasses all of the PRD elements formed a complex with not only one but two p50 homodimers (Fig. 6A, lanes 1 to 3). Dissecting their location by mutating the three G-rich stretches, we confirmed that the κB site recruited one p50 homodimer (Fig. 6A, lanes 4 to 9), but that the central triple-G (3-G) element within the IREs recruited a second p50 homodimer (Fig. 6A, lanes 10 to 18). Although this triple-G element is not required for binding to IRFs, it is evolutionarily conserved (*45*).

To explore the functional consequence of these binding events, we constructed a mathematical model of the abundance of *IFN*β mRNA, in which the thermodynamic formulation of promoter activity *f* (Fig. 6B) was embedded in a differential equation that described mRNA production and decay. Simulations showed that this model predicted a substantial differential responsiveness of *IFN*β to stimulation by CpG and LPS in wild-type, but not p50KO, cells (Fig. 6C). Indeed, our experimental analysis revealed that whereas wild-type cells did not exhibit expression of *IFN*β in response to CpG, p50KO cells showed substantial misexpression (Fig. 6D).

Because IFN-β coordinates a large antiviral gene expression program through the activation of ISGF3, we examined how stimulus-specific gating of the *IFN*β enhancer by p50-p50 might affect downstream responses (Fig. 7A). We characterized the LPS- and CpG-induced profiles of ISGF3 activation and found inappropriate induction of ISGF3 in response to CpG in p50KO macrophages (Fig. 7B), whereas IRF3 was not activated (fig. S7). Furthermore, in p50KO macrophages, CpG induced the expression of known antiviral genes (Fig. 7C) and IFN response genes that were revealed by microarray studies (Fig. 7D). We established a viral infection assay in which the priming of macrophages by IFN-β inhibited the infectivity of a green fluorescent protein (GFP)–expressing cytomegalovirus (CMV) (*46*), whereas macrophages defective in IFN signaling were more susceptible than wild-type cells to infection (fig. S8). Exposing macrophages to LPS rendered them more resistant than untreated cells to infection by CMV, whereas exposure to CpG did not (Fig. 7, E and F), which reflected the stimulus-specific production of IFN-β. Such stimulus specificity in the mounting of resistance to viral infection was severely compromised in p50KO macrophages because CpG also resulted in increased antiviral resistance in these cells. Our results may relate to the resistance of *nfkb1*$^{-/-}$ mice to encephalomyocarditis virus (EMCV) (*26*) and to

that of an *nfkb1*$^{-/-}$ immortalized fibroblast cell line to influenza (*47*). Given the cytostatic or even cytotoxic effects of IFNs, stimulus-restricted production of IFN-β is important for the health of cells and organisms. Whereas CpG promoted cell proliferation in wild-type macrophages, in p50KO macrophages it caused cytotoxicity as a detrimental consequence of an overactive antiviral immune program (Fig. 7G).

DISCUSSION

Our findings have revealed unexpected cross-regulation between the two primary transcription factors that coordinate innate immune responses. Whereas the NF-κB and IRF activators bind to their respective cognate sites (κB and IRE, respectively), we report that the NF-κB p50-p50 repressor binds to and regulates a subset of IREs, termed G-IREs, whose sequence contains or is in direct vicinity to a 3-G sequence. We show that p50 homodimers, as an abundant constitutive component of the nucleus, have substantial thresholding functions for the expression of IRF-responsive genes. Exemplified by the combinatorial *IFN*β enhancer, our work emphasizes the importance of homeostatic repressors in restricting gene expression to specific stimuli by binding to sites that overlap with those of stimulus-inducible factors.

By combining unbiased gene expression phenotyping studies of *nfkb1*$^{-/-}$ cells with biochemical and molecular biological studies, we provided evidence in vitro and in cells that NF-κB p50 homodimers directly regulate G-IRE–containing promoters. However, indirect mechanisms, such as the enhanced production of autocrine type I IFN or the regulation of ERK by p105 (the precursor form of p50), may contribute to the gene expression phenotype and may provide an explanation for the enhanced activation of genes in whose proximal regulatory regions (−1 to +0.3 kb) we did not find a G-rich sequence flanking an IRE. That IFN-responsive ISGF3 was not enhanced in activation in p50KO cells in response to LPS (Fig. 7B), but that the increased expression of genes was observed at 1 hour after LPS stimulation (Fig. 1, C and D) (before the activation of ISGF3), and that many G-IRE–containing genes showed enhanced responsiveness to ectopic IFN stimulation (fig. S1) corroborates our conclusion that p50 regulates G-IRE–containing promoters directly.

The sequence-specific interaction of transcription factors with their specific DNA binding sites is an organizing principle for understanding the logic of gene regulatory circuits. Sequence specificity has traditionally

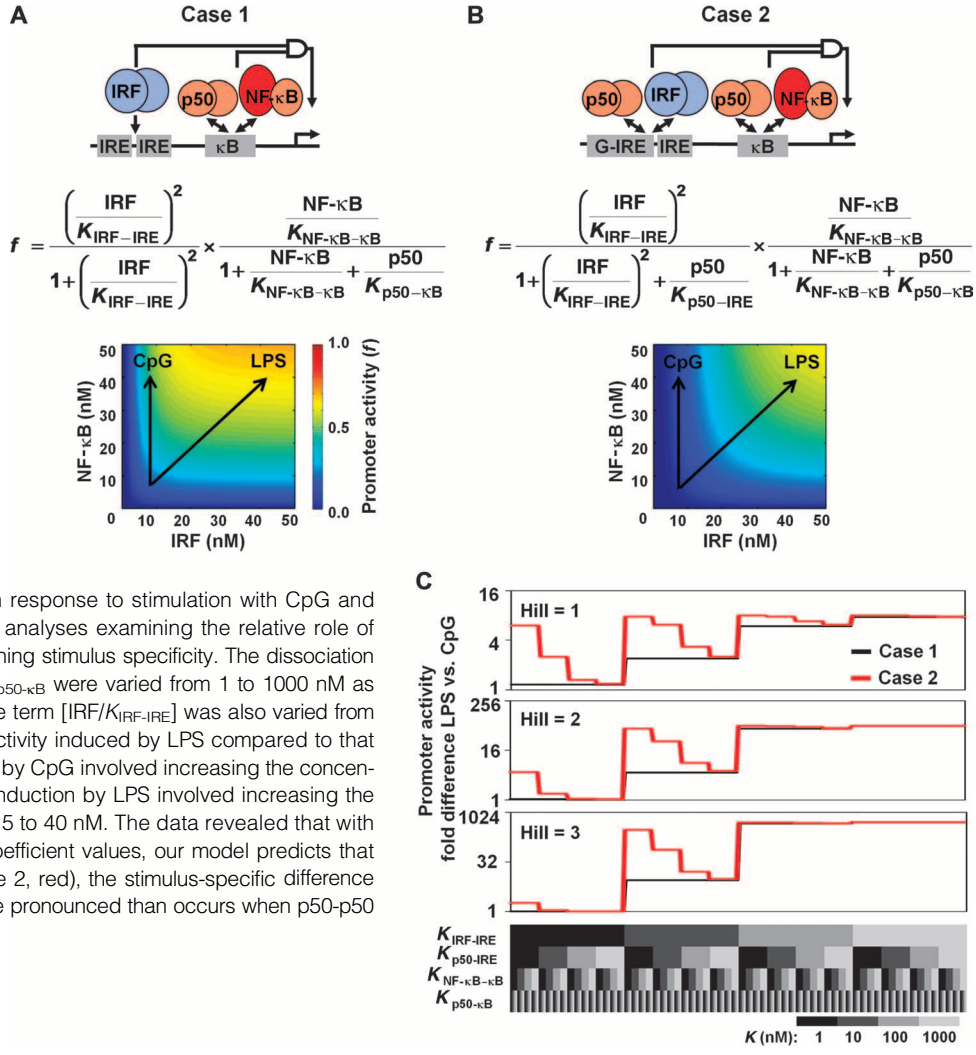

Fig. 5. Mathematical modeling predicts that interactions between p50-p50 and G-IRE serve to enforce the stimulus specificity of AND-gate promoters. (**A**) Schematic thermodynamic formulation and computational determination of the activity (*f*) of an AND-gate promoter that is a function of synergistic IRF and NF-κB concentrations and of the competitive repression of the κB site by p50-p50. The arrows indicate how the concentrations of active NF-κB alone or of NF-κB and IRF may increase in response to stimulation with CpG and LPS, respectively. (**B**) Schematic thermodynamic formulation and computational determination of the activity (*f*) of an AND-gate promoter that is a function of synergistic IRF and NF-κB concentrations and competitive repression of both the G-IRE and the κB site by p50-p50. Analogous to (A), the arrows indicate how the concentrations of active NF-κB alone or of NF-κB and IRF may increase in response to stimulation with CpG and LPS, respectively. (**C**) Parameter sensitivity analyses examining the relative role of the four dissociation constants (*K*) in determining stimulus specificity. The dissociation constants $K_{IRF\text{-}IRE}$, $K_{p50\text{-}IRE}$, $K_{NF\text{-}\kappa B\text{–}\kappa B}$, and $K_{p50\text{-}\kappa B}$ were varied from 1 to 1000 nM as indicated (bottom). The Hill coefficient for the term [IRF/$K_{IRF\text{-}IRE}$] was also varied from 1 to 3. The fold difference in the promoter activity induced by LPS compared to that by CpG was plotted on the *y* axis. Induction by CpG involved increasing the concentration of NF-κB from 5 to 40 nM, whereas induction by LPS involved increasing the concentrations of both IRF and NF-κB from 5 to 40 nM. The data revealed that with a wide range of binding affinities and Hill coefficient values, our model predicts that when p50-p50 is bound to the IRE site (case 2, red), the stimulus-specific difference in promoter activity (LPS versus CpG) is more pronounced than occurs when p50-p50 is not bound to the IRE site (case 1, black).

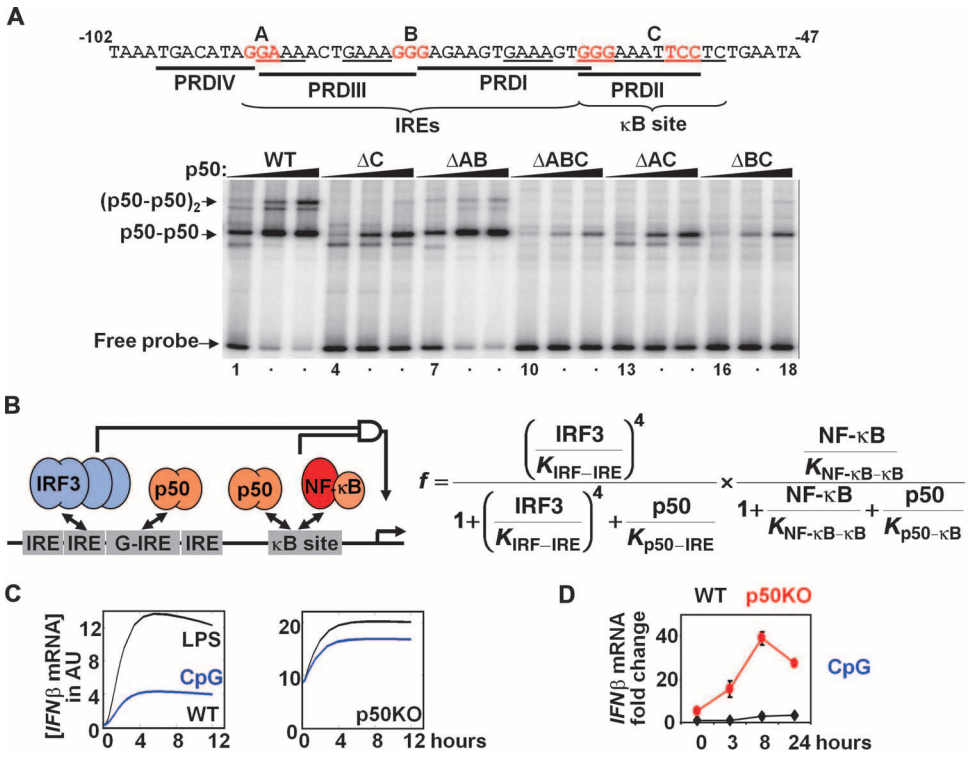

Fig. 6. Stimulus-specific expression of *IFN*β is enforced by the binding of p50 to a G-IRE within the enhancer of *IFN*β. (**A**) DNA binding activity of p50-p50 on the *IFN*β enhancer (from −102 to −47). The indicated IRE and κB site mutants were used in EMSAs with 10, 50, and 100 ng of recombinant p50 protein. Mutants (designated with Δ) had the indicated trinucleotides in red mutated to "TCT" (for GGA or GGG) or "AGA" (for TCC). (**B**) A schematic illustrating the regulation of the *IFN*β enhancer by p50-p50 on both the G-IRE and the κB sites. A thermodynamic formulation of the fractional promoter activity *f*. (**C**) Computational simulations of the abundance of *IFN*β mRNA with a kinetic model driven by the fractional promoter activity *f* in WT and p50KO cells in response to LPS (black) or CpG (blue). (**D**) RT-qPCR determination of the fold change in the abundance of *IFN*β mRNA in WT (black) BMDMs compared to that in p50KO BMDMs (red) following stimulation with CpG (100 nM) for the indicated times. Data are from, or representative of, at least three experiments.

been determined by low-throughput biochemical assays or polymerase chain reaction (PCR)–mediated DNA selection schemes that identify the highest-affinity DNA sequences (*48*). However, unbiased ChIP-chip or ChIP-seq experiments have revealed the association of transcription factors with DNAs that do not contain known cognate sequences, although indirect binding cannot be ruled out (*49*, *50*). High-throughput biochemical affinity measurements in miniaturized assay systems have, however, revealed that some transcription factors have much broader binding specificity than was anticipated or that they may have more than one mode of specific DNA binding (*51*–*54*). These observations set the stage for overlap in the sequence space that is associated with different transcription factor families. Competitive binding between specific IRF and NF-κB family members is an example of this scenario that has important gene regulatory consequences. Our study suggests that DNA elements have evolved to recruit two distinct DNA binding proteins to achieve specific regulation of gene expression; such hybrid elements may not be uniquely assigned as a response element of a single signaling pathway. In the case of G-IREs, we classify these sequences as a subclass of IREs, rather than of κB sites, because the G-IRE conforms to the direct repeat character of IREs, unlike the palindromic κB site, and IRFs are the cognate transcriptional activators, whereas the NF-κB family member p50-p50 appears to function as a competitive repressor.

Delineating the specificity of transcriptional regulators remains challenging. High-throughput, cell-free biochemical approaches characterize the capacity of DNA binding domains to bind to particular sequences but are dependent on precise reaction conditions and the quality of the recombinant protein (*51*–*54*). We used high-throughput gene expression measurements in genetically altered cells to identify candidate interactions that were functional (Fig. 1). Biochemical studies confirmed the capacity of the p50-p50 homodimer to bind to G-IREs and to repress IRF-driven transcription (Fig. 2). Biophysical considerations based on related x-ray structures rationalized the biophysical basis for the ability of p50-p50 to bind to a 3-G motif without requiring a second palindromic half-site, namely, high-affinity interactions by one p50 monomer and a flexible hinge between the DNA binding and the dimerization domains within the other monomer (Fig. 3). In contrast, the ubiquitous NF-κB p50-p65 dimer did not form a complex on G-IRE probes (Fig. 1E). Previous crystallographic studies revealed the formation of fewer hydrogen bonds by p65 than by p50 with a single half-site, which is suggestive of lower-affinity binding (*55*), and future studies should address whether the hinge of p65 is not as flexible as that of p50. However, the identity of the IRF family member with which p50-p50 competes with is less unambiguous. We observed the gene expression phenotype in p50KO cells at early time points after exposure to LPS (Fig. 1, C and D, and fig. S2), correlating with the activation profile of IRF3 (30 min to 2 hours) rather than with that of ISGF3 (2 to 6 hours) (Fig. 1E). Furthermore, the phenotype of p50KO cells in response to IFN-β, which only activates ISGF3, was more modest than that in response to LPS (fig. S1). Recent protein binding microarray experiments revealed that IRF3 prefers IRE sequences that contain "GG"AAAC, whereas the ISGF3 complex prefers the IRE sequence "TG"AAAC (*54*). Hence, we speculate that p50-p50 bound to G-IREs functions primarily as a competitor of IRF3 and, to a lesser extent, of the ISGF3 complex.

Through mathematical modeling, we have begun to explore what the functional consequences of p50-p50–IRE cross-binding may be within gene regulatory circuits. Combinatorial regulation by sequence-specific transcription factors is thought to form the basis for stimulus-specific gene expression (*40*, *56*, *57*). Mathematically, such regulation has been described with Boolean logic gates (*58*, *59*), but such studies presume stimulus-responsive transcription factors that have no or negligible basal activity. However, in mammalian cells, even highly stimulus-responsive tran-

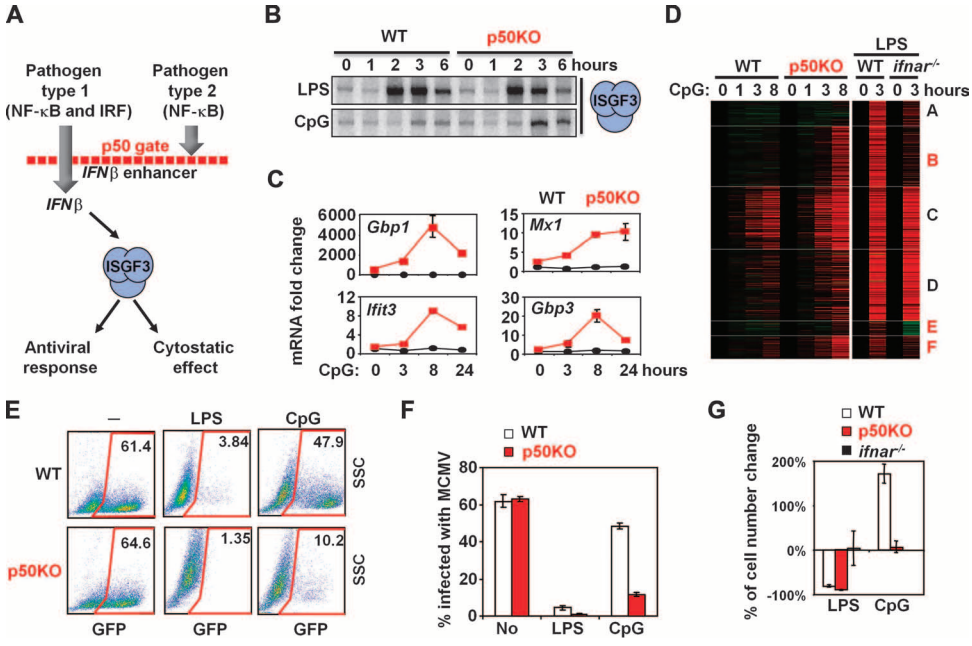

Fig. 7. p50 restricts antiviral, and potentially detrimental, gene expression to IRF-inducing stimuli. (**A**) Schematic of pathogen-specific activation of the *IFNβ* enhancer; gating by p50-p50 enables only certain pathogens (those that can stimulate both NF-κB and IRF) to activate antiviral responses, ensuring that the cytostatic effects of IFN signaling remain shut off when antiviral responses are not needed. (**B**) Nuclear ISGF3 activities in response to LPS (0.1 μg/ml) or CpG (100 nM) were revealed by EMSAs of nuclear extracts from WT and p50KO BMDMs. (**C**) Fold changes in the abundances of mRNAs of IFN-β–inducible genes were determined by RT-qPCR analysis of WT (black) and p50KO (red) BMDMs stimulated with CpG (100 nM) for the indicated times. (**D**) Microarray gene expression profiles of WT and p50KO BMDMs that were left unstimulated or were stimulated with CpG (100 nM) for 3, 8, or 24 hours, together with microarray expression profile of WT and *ifnar*$^{-/-}$ BMDMs that were left unstimulated or were stimulated with LPS (0.1 μg/ml) for 3 hours, were analyzed by *K*-means clustering. Cluster identifiers are indicated on the right. Red indicates IFN-β– and IFNAR-dependent clusters. (**E**) Induction of antiviral resistance after priming treatments. After a 24-hour treatment with PBS ("–"), LPS (0.1 μg/ml), or CpG (100 nM), WT and p50KO BMDMs were infected with MCMV-GFP. Forty-eight hours later, productively infected cells expressing GFP were quantified (red gate) by flow cytometry (side scatter versus GFP). (**F**) The percentage of infected WT (white) or p50KO (red) BMDMs expressing GFP in (E) were plotted as averages from triplicate determinations. The data are representative of three independent experiments. (**G**) Percentage changes in cell numbers of WT (white), p50KO (red), and *ifnar*$^{-/-}$ (black) BMDMs after they were stimulated with LPS (0.1 μg/ml) or CpG (100 nM) relative to those of untreated cells were determined by crystal violet assay. Error bars represent the SD from three biological replicates. Data are from, or representative of, at least three experiments.

scription factors such as NF-κB and IRF3 or ISGF3 show detectable basal activities; indeed, Western blotting analysis indicated that as much as 30% of IRF3 may have been constitutively nuclear (fig. S7), although not all of it was likely to be active. A thermodynamic formulation of an AND-gate described the dose-response behavior of NF-κB and IRF and revealed that such basal activity rendered the AND-gate leaky; specifically, stimuli such as CpG that activate NF-κB but not IRF will nevertheless result in appreciable AND-gate promoter activity. In this context, the binding of the constitutive repressor p50-p50 to IREs functions as a gatekeeper of combinatorial AND-gate promoters. In addition to the presumed synergistic interactions of coordinated transcription factors, our combined computational-experimental study of IFN-β suggests that such a gating mechanism is critical for enforcing stimulus specificity in gene expression and the subsequent antiviral responses.

More broadly, in the context of basal activities of transcription factors, the mechanisms that restrict transcriptional responses to appropriate stimuli or enforce strict synergy requirements remain incompletely understood. Chromatin regulation provides a means for regulating the accessibility of transcriptional activator–binding sites and has also been proposed to provide thresholding functions (*60*). However, the thresholding function of competitive binding by p50-p50 may not introduce the type of delay that chromatin-opening steps may require. In addition, the thresholding function may be tunable, because the homeostatic abundance of p50 may be regulated to control the responsiveness of the IFN program. Indeed, prolonged activation of NF-κB resulted in increased amounts of p50 and enhanced binding of p50-p50 to IREs (Fig. 1E), and this may further restrict the IFN response to a narrow set of stimuli without affecting the kinetics of activation.

Understanding the role of homeostatic thresholding factors in stimulus-responsive gene control is critical for the development of therapeutic strategies that are based on the manipulation of gene expression responses. In harnessing the IFN response for antiviral and anticancer treatment, our study suggests that the cross-regulatory functions of the p50-p50 may limit the efficacy of IFN treatment. However, an understanding of the promoter-gating function of p50-p50 holds promise for tuning the specificity of adaptive immune adjuvants and innate immune priming strategies.

MATERIALS AND METHODS

Cell culture

BMDMs were isolated from C57BL/6, *nfkb1*$^{-/-}$, *ifnar*$^{-/-}$, and *p105*$^{-/-}$ mice and were cultured in L929 cell–conditioned medium for 5 to 8 days. Primary MEFs were prepared with E12 (embryonic day 12) to E14 embryos from C57BL/6 and *nfkb1*$^{-/-}$ mice and were cultured in Dulbecco's modified Eagle's medium (DMEM) containing 10% bovine calf serum for five to six passages. Human embryonic kidney (HEK) 293T cells that were stably transfected with plasmids encoding human TLR4a, MD2, and CD14 (InvivoGen) are referred to as TLR4–HEK 293T cells. Cells were stimulated with LPS (0.1 mg/ml; Sigma, B5:055), CpG (100 nM;

ODN 1668, InvivoGen), and murine IFN-β [10 U/ml (for BMDMs) or 2500 U/ml (for MEFs); Biogen Inc.]. A higher concentration of IFN-β was used for MEFs because they exhibit lower responsiveness to IFN than do macrophages.

Transcriptome and bioinformatic analysis

RNA was extracted from cells with the Qiagen RNeasy kit and hybridized to Illumina Mouse RefSeq Sentrix-8 V1.1 and V2 BeadChips or CodeLink Uniset 1 mouse (GE Healthcare) microarrays at the University of California–San Diego Biogem facility. De novo motif searches were performed with the promoter sequences 1 kb upstream and 0.5 kb downstream of the transcription start site with the motif search program Homer developed by C. Benner (*61*). An in-depth description and benchmarking of this software suite can be found at http://biowhat.ucsd.edu/homer/. We extracted RNA from littermate wild-type and *nfkb1*$^{-/-}$ MEFs that were unstimulated or stimulated with LPS (0.1 μg/ml) for 1, 3, or 8 hours; from *crel*$^{-/-}$*p65*$^{-/-}$ MEFs that were left unstimulated or were stimulated with LPS (0.1 μg/ml) for 1, 3, or 8 hours; and from wild-type MEFs that were left unstimulated or were stimulated with LPS (0.1 μg/ml) (three biological repeated samples), tumor necrosis factor (TNF; 10 ng/ml), platelet-derived growth factor BB (PDGFBB; 50 ng/ml), and IFN-β (2500 U/ml) for 1, 3, or 8 hours. RNAs were hybridized to Illumina mouse RefSeq Sentrix-8 V1.1 BeadChip arrays. Probes with ≥2-fold change in expression under any stimulus conditions in wild-type cells were selected. *K*-means clustering was performed with selected probes on all of the wild-type samples (TNF, IFN-β, PDGFBB, and the three LPS data sets) and on the *crel*$^{-/-}$*p65*$^{-/-}$ samples that were stimulated with LPS. The LPS-treated *nfkb1*$^{-/-}$ data set was matched to the final clusters, and the average fold change in expression for each gene cluster was calculated and shown next to the heat map in Fig. 1C. RNA from littermate wild-type and *nfkb1*$^{-/-}$ BMDMs that were stimulated with LPS (0.1 μg/ml), IFN-β (10 U/ml), or CpG (100 nM) for 1, 3, or 8 hours was hybridized to Illumina mouse RefSeq Sentrix-8 V2 BeadChip arrays. Raw expression data were normalized to several unstimulated control data sets. Probes with ≥$2^{1.2}$-fold (that is, ≥2.97-fold) change in expression at any point of the LPS time course were selected. Fold changes in expression from multiple probes for a single gene (accession number) were averaged. *K*-means clustering was performed with wild-type (LPS), p50KO (LPS), wild-type (IFN-β), and *infar*$^{-/-}$ (LPS) time course data sets and shown in Figs. 1D and 7D and fig. S1. All of the array data shown are available in the NCBI Gene Expression Omnibus database with the accession number GSE27112.

Expression phenotype of p50KO BMDMs and classification of G-rich IREs

Microarray data [CodeLink Uniset 1 Mouse (GE Healthcare) microarrays] were derived from wild-type and *nfkb1*$^{-/-}$ BMDMs stimulated with LPS (0.1 μg/ml) for 6 hours (two biological replicates), wild-type BMDMs stimulated with IFN-β (100 U/ml), and *infar*$^{-/-}$ BMDMs stimulated with LPS (0.1 μg/ml). Genes with ≥2-fold change in expression under any condition were subjected to *K*-means clustering. One hundred seven genes that were IFN-β–inducible and showed IFNAR dependence when induced by LPS were selected and are shown in table S1. The expression profiles of these genes in p50KO cells in response to LPS (Fig. 2B) were determined with replicate microarray data from wild-type and *nfkb1*$^{-/-}$ BMDMs stimulated with LPS (0.1 μg/ml) and statistical analysis with Vampire (*62*). IREs were classified as G-rich or non–G-rich by examining the IRE-binding sites 1 kb upstream and 0.5 kb downstream of the transcription start site. Sequences were downloaded from the UCSC (University of California, Santa Cruz) Genome Browser (Mouse February 2006 assembly; NCBI36/mm8) with the UCSC known genes track, which are based on the annotation from UniProt, RefSeq, and GenBank mRNAs. IRE sites were identified with MatInspector software (Release Professional 7.7.3, February 2008) (*63*) with the following parameters: Matrix Family Library Version 7.0 (October 2007), the family of matrices V$IRFF (includes the matrices V$ISRE.01, V$IRF1.01, V$IRF2.01, V$IRF3.01, V$IRF4.01, and V$IRF7.01), and the optimized matrix similarity threshold (the number of false-positive matches found in nonregulatory test sequences is minimized) of 0.88. IREs containing GGGN, GAGG, or GTGG motifs within 7 base pairs (bp) from the 5′ end of the IRE element ("G/A/T"AAA or "A"ANNGAAA) were considered to be G-rich IREs, as indicated in table S1.

Biochemical assays

Western blotting analysis and EMSAs were conducted with standard methods as described previously (*64*, *65*). For Western blotting analysis, supershift assays, and ChIP assays, we used antibodies against p65 (Santa Cruz Biotechnology, sc-372), p50 (sc-114), STAT2 (sc-950), α-tubulin (sc-5286), p50 (N. Rice, NC-1263), lamin A/C (Cell Signaling, #2032), and IRF3 (Cell Signaling, #4962). The EMSA probes used in this study are listed in table S2. The primers that were used for ChIP assays are listed in table S3, whereas the primers that were used for quantitative RT-qPCR assays are listed in table S4. G-rich and non–G-rich IRE sequences in luciferase reporter constructs were as follows (IREs are underlined): G-rich IRE, TCGACGGGAAAGGGAAAGGGAAAGGGAAAGGGAAAGGGAAAG; non–G-rich IRE, TCGACAAGAAAAAGAAAAAGAAAAAGAAAAAGAAAAAGAAAAAG. Total RNA was isolated from BMDMs or MEFs and treated as indicated with the Qiagen RNeasy kit. RNA was reverse-transcribed with SuperScript II Reverse Transcriptase (Invitrogen), and the resulting complementary DNA (cDNA) was used for real-time qPCR (RT-qPCR) analysis with SYBR Green. ChIP assays were conducted as previously described (*66*, *67*). Briefly, BMDMs were stimulated and fixed with 1% formaldehyde. Cross-linked pellets were sonicated to obtain DNA fragments of 300 to 800 bp and incubated with antibody overnight. Immunoprecipitated DNA fragments were subjected to reverse cross-linking, purified, and amplified by qPCR. Reporter assays were conducted by transfecting TLR4–HEK 293T cells plated in 24-well plates with 40 ng of the indicated IRE luciferase reporter construct and 40, 120, or 300 ng of plasmid encoding p50 or the p50 DBD mutant (R56A,Y57A) with Lipofectamine 2000 (Invitrogen). Forty-eight hours after transfection, cells were stimulated with LPS (0.1 μg/ml) for 6 hours, and luciferase units were measured by standard methodology with the Dual-Luciferase Reporter Assay System (Promega). IRE luciferase activities were normalized to those of β-galactosidase as measured by the Galacto-Light Plus System (Applied Biosystems).

Computational modeling

Thermodynamic formulations of promoter activity *f* are shown in the figures and are based on previous work (*37*, *41*). Thermodynamic models of promoter–transcription factor interactions used parameter values that were based on measurements and reasonable estimates. The amount of nuclear p50-p50 was estimated to be about 30,000 dimers (Fig. 1B). On the basis of the volumes of macrophages and their nuclei as measured by us and others (*68*, *69*) to be 1 to 2 pl and 0.15 to 0.3 pl, respectively, we estimated the molar concentration of p50-p50 to be at least 200 nM. To ensure that our modeling results were conservative, we also considered lower concentrations of p50-p50. The stimulus-induced concentration of nuclear NF-κB was determined to peak at about 100 nM (*64*). The stimulus-induced concentration of IRF peaked at 100 nM, with a basal concentration of 10 nM. The dissociation constants were reasonably estimated according to simple guidelines: NF-κB p50-p65 has

a higher affinity for κB sites than that of p50-p50 (that is, $K_{\text{NF-κB–κB}} < K_{\text{p50-κB}}$); IRF has a higher affinity for IREs than that of p50-p50 (that is, $K_{\text{IRF-IRE}} < K_{\text{p50-IRE}}$); the affinity of NF-κB p50-p65 for κB sites is higher than that of IRFs for IREs (that is, $K_{\text{NF-κB–κB}} < K_{\text{IRF-IRE}}$); and p50-p50 has a higher affinity for κB sites than for IREs (that is, $K_{\text{p50-κB}} < K_{\text{p50-IRE}}$). The specific parameter values were as follows: for Fig. 4, E and F: [p50-p50] = 100 nM, [IRF] = 1 to 100 nM, $K_{\text{IRF-IRE}}$ = 10 nM, $K_{\text{p50-IRE}}$ = 100 nM (Fig. 4E) or 10 to 1000 nM (Fig. 4F); for Fig. 5, A and B: [p50-p50] = 100 nM, [IRF] = 0 to 50 nM, [NF-κB p65-p50] = 0 to 50 nM, $K_{\text{IRF-IRE}}$ = 5 nM, $K_{\text{p50-IRE}}$ = 10 nM, $K_{\text{p50-κB}}$ = 5 nM, $K_{\text{NFκB-κB}}$ = 1 nM; for Fig. 5C, parameter sensitivity analyses were performed by varying the binding dissociation constants $K_{\text{IRF-IRE}}$, $K_{\text{p50-IRE}}$, $K_{\text{p50-κB}}$, and $K_{\text{NFκB-κB}}$ from 1 to 1000 nM as indicated in the figure. The Hill coefficient for the term [IRF/$K_{\text{IRF-IRE}}$] was also varied from 1 to 3. The kinetic model of the abundance of *IFN*β mRNA (r) was modeled by the ordinary differential equation:

$$\frac{dr}{dt}(t) = k_{\text{i}} f - k_{\text{d}} r$$

where k_{i} is the mRNA synthesis rate constant [in arbitrary units (AUs) of mRNA concentration min^{-1}] and k_{d} is the mRNA degradation rate constant (in min^{-1}). For Fig. 6, B and C, the thermodynamic model for f had the following parameters: $K_{\text{IRF-IRE}}$ = 5 nM, $K_{\text{p50-IRE}}$ = 10 nM, $K_{\text{p50-κB}}$ = 5 nM, $K_{\text{NF-κB–κB}}$ = 1 nM, and [p50-p50] = 100 nM. The time-dependent inputs of the model were as follows: basal [NF-κB] = 1 nM; in response to LPS and CpG, [NF-κB] was 10, 50, 40, or 30 nM at 30, 120, 360, and 720 min, respectively; basal [IRF] = 7.5 nM; in response to LPS, [IRF] was 20, 50, 40, or 20 nM at 30, 120, 360, and 720 min, respectively, and these concentrations were estimated from gel shift experiments and Western blotting analysis of nuclear extracts. The half-life of *IFN*β mRNA was estimated at 1 hour, which resulted in a degradation rate constant k_{d} of 0.0116 min^{-1}. The mRNA synthesis rate constant k_{i} was arbitrarily set to 0.24 AU min^{-1}. Simulations were performed with the numerical solver of the MATLAB ode23 function.

Viral infections

Before infections, BMDMs were seeded into 24-well plates, allowed to adhere, and treated with the indicated stimuli for 24 hours. BMDMs were infected with live murine CMV (MCMV)–GFP and were analyzed for the presence of GFP after 48 hours by flow cytometry.

SUPPLEMENTARY MATERIALS

www.sciencesignaling.org/cgi/content/full/4/161/ra11/DC1

Fig. S1. Expression profiling of IFN-β responses reveals the enhanced expression of some genes at early time points.

Fig. S2. The gene expression phenotype observed in p50KO cells depends on the absence of p50 and not the absence of p105.

Fig. S3. The DNA binding activities of transcriptional activators and the p50-p50 repressor in response to LPS.

Fig. S4. STAT2 is recruited to IRE sequences irrespective of whether they are G-rich.

Fig. S5. Increased expression of p50 protein reduced IRF-mediated activation of G-rich IRE–driven reporter gene, but not non–G-rich IRE–driven reporter gene.

Fig. S6. G-rich IREs are more likely than non–G-rich IREs to exhibit enhanced basal expression in p50-deficient BMDMs.

Fig. S7. IRF3 is not activated in response to CpG in either WT or p50KO BMDMs.

Fig. S8. Assays of infection of cells by MCMV-GFP reveal IFN-β–mediated antiviral responses.

Table S1. IFN response genes.

Table S2. List of EMSA probes.

Table S3. List of the primers used for ChIP assays.

Table S4. List of the primers used for RT-qPCR assays.

REFERENCES AND NOTES

1. O. Takeuchi, S. Akira, Pattern recognition receptors and inflammation. *Cell* **140**, 805–820 (2010).
2. G. J. Nau, J. F. Richmond, A. Schlesinger, E. G. Jennings, E. S. Lander, R. A. Young, Human macrophage activation programs induced by bacterial pathogens. *Proc. Natl. Acad. Sci. U.S.A.* **99**, 1503–1508 (2002).
3. S. Doyle, S. Vaidya, R. O'Connell, H. Dadgostar, P. Dempsey, T. Wu, G. Rao, R. Sun, M. Haberland, R. Modlin, G. Cheng, IRF3 mediates a TLR3/TLR4-specific antiviral gene program. *Immunity* **17**, 251–263 (2002).
4. S. Ogawa, J. Lozach, C. Benner, G. Pascual, R. K. Tangirala, S. Westin, A. Hoffmann, S. Subramaniam, M. David, M. G. Rosenfeld, C. K. Glass, Molecular determinants of crosstalk between nuclear receptors and toll-like receptors. *Cell* **122**, 707–721 (2005).
5. S. L. Foster, D. C. Hargreaves, R. Medzhitov, Gene-specific control of inflammation by TLR-induced chromatin modifications. *Nature* **447**, 972–978 (2007).
6. C. Nathan, Points of control in inflammation. *Nature* **420**, 846–852 (2002).
7. T. Decker, M. Müller, S. Stockinger, The yin and yang of type I interferon activity in bacterial infection. *Nat. Rev. Immunol.* **5**, 675–687 (2005).
8. A. Marshak-Rothstein, Toll-like receptors in systemic autoimmune disease. *Nat. Rev. Immunol.* **6**, 823–835 (2006).
9. J. C. Roach, K. D. Smith, K. L. Strobe, S. M. Nissen, C. D. Haudenschild, D. Zhou, T. J. Vasicek, G. A. Held, G. A. Stolovitzky, L. E. Hood, A. Aderem, Transcription factor expression in lipopolysaccharide-activated peripheral-blood-derived mononuclear cells. *Proc. Natl. Acad. Sci. U.S.A.* **104**, 16245–16250 (2007).
10. S. A. Ramsey, S. L. Klemm, D. E. Zak, K. A. Kennedy, V. Thorsson, B. Li, M. Gilchrist, E. S. Gold, C. D. Johnson, V. Litvak, G. Navarro, J. C. Roach, C. M. Rosenberger, A. G. Rust, N. Yudkovsky, A. Aderem, I. Shmulevich, Uncovering a macrophage transcriptional program by integrating evidence from motif scanning and expression dynamics. *PLoS Comput. Biol.* **4**, e1000021 (2008).
11. G. Oganesyan, S. K. Saha, B. Guo, J. Q. He, A. Shahangian, B. Zarnegar, A. Perry, G. Cheng, Critical role of TRAF3 in the Toll-like receptor-dependent and -independent antiviral response. *Nature* **439**, 208–211 (2006).
12. I. Amit, M. Garber, N. Chevrier, A. P. Leite, Y. Donner, T. Eisenhaure, M. Guttman, J. K. Grenier, W. Li, O. Zuk, L. A. Schubert, B. Birditt, T. Shay, A. Goren, X. Zhang, Z. Smith, R. Deering, R. C. McDonald, M. Cabili, B. E. Bernstein, J. L. Rinn, A. Meissner, D. E. Root, N. Hacohen, A. Regev, Unbiased reconstruction of a mammalian transcriptional network mediating pathogen responses. *Science* **326**, 257–263 (2009).
13. S. Akira, K. Takeda, Toll-like receptor signalling. *Nat. Rev. Immunol.* **4**, 499–511 (2004).
14. S. Akira, S. Uematsu, O. Takeuchi, Pathogen recognition and innate immunity. *Cell* **124**, 783–801 (2006).
15. R. Medzhitov, Origin and physiological roles of inflammation. *Nature* **454**, 428–435 (2008).
16. T. Kawai, S. Akira, The role of pattern-recognition receptors in innate immunity: Update on Toll-like receptors. *Nat. Immunol.* **11**, 373–384 (2010).
17. S. Sharma, B. R. tenOever, N. Grandvaux, G. P. Zhou, R. Lin, J. Hiscott, Triggering the interferon antiviral response through an IKK-related pathway. *Science* **300**, 1148–1151 (2003).
18. Y. Fujii, T. Shimizu, M. Kusumoto, Y. Kyogoku, T. Taniguchi, T. Hakoshima, Crystal structure of an IRF–DNA complex reveals novel DNA recognition and cooperative binding to a tandem repeat of core sequences. *EMBO J.* **18**, 5028–5041 (1999).
19. A. Hoffmann, G. Natoli, G. Ghosh, Transcriptional regulation via the NF-κB signaling module. *Oncogene* **25**, 6706–6716 (2006).
20. S. Sanjabi, A. Hoffmann, H. C. Liou, D. Baltimore, S. T. Smale, Selective requirement for c-Rel during IL-12 P40 gene induction in macrophages. *Proc. Natl. Acad. Sci. U.S.A.* **97**, 12705–12710 (2000).
21. A. Hoffmann, T. H. Leung, D. Baltimore, Genetic analysis of NF-κB/Rel transcription factors defines functional specificities. *EMBO J.* **22**, 5530–5539 (2003).
22. S. M. Kang, A. C. Tran, M. Grilli, M. J. Lenardo, NF-κB subunit regulation in nontransformed $CD4^+$ T lymphocytes. *Science* **256**, 1452–1456 (1992).
23. R. M. Ten, C. V. Paya, N. Israel, O. Le Bail, M. G. Mattei, J. L. Virelizier, P. Kourilsky, A. Israel, The characterization of the promoter of the gene encoding the p50 subunit of NF-κB indicates that it participates in its own regulation. *EMBO J.* **11**, 195–203 (1992).
24. D. Plaksin, P. A. Baeuerle, L. Eisenbach, KBF1 (p50 NF-κB homodimer) acts as a repressor of H-2Kb gene expression in metastatic tumor cells. *J. Exp. Med.* **177**, 1651–1662 (1993).
25. H. C. Ledebur, T. P. Parks, Transcriptional regulation of the intercellular adhesion molecule-1 gene by inflammatory cytokines in human endothelial cells. Essential roles of a variant NF-κB site and p65 homodimers. *J. Biol. Chem.* **270**, 933–943 (1995).
26. W. C. Sha, H. C. Liou, E. I. Tuomanen, D. Baltimore, Targeted disruption of the p50 subunit of NF-κB leads to multifocal defects in immune responses. *Cell* **80**, 321–330 (1995).

27. I. A. Udalova, A. Richardson, A. Denys, C. Smith, H. Ackerman, B. Foxwell, D. Kwiatkowski, Functional consequences of a polymorphism affecting NF-κB p50-p50 binding to the TNF promoter region. *Mol. Cell. Biol.* **20**, 9113–9119 (2000).
28. J. Bohuslav, V. V. Kravchenko, G. C. Parry, J. H. Erlich, S. Gerondakis, N. Mackman, R. J. Ulevitch, Regulation of an essential innate immune response by the p50 subunit of NF-κB. *J. Clin. Invest.* **102**, 1645–1652 (1998).
29. H. C. Liou, G. P. Nolan, S. Ghosh, T. Fujita, D. Baltimore, The NF-κB p50 precursor, p105, contains an internal IκB-like inhibitor that preferentially inhibits p50. *EMBO J.* **11**, 3003–3009 (1992).
30. M. R. Waterfield, M. Zhang, L. P. Norman, S. C. Sun, NF-κB1/p105 regulates lipopolysaccharide-stimulated MAP kinase signaling by governing the stability and function of the Tpl2 kinase. *Mol. Cell* **11**, 685–694 (2003).
31. S. Beinke, J. Deka, V. Lang, M. P. Belich, P. A. Walker, S. Howell, S. J. Smerdon, S. J. Gamblin, S. C. Ley, NF-κB1 p105 negatively regulates TPL-2 MEK kinase activity. *Mol. Cell. Biol.* **23**, 4739–4752 (2003).
32. M. Chang, A. J. Lee, L. Fitzpatrick, M. Zhang, S. C. Sun, NF-κB1 p105 regulates T cell homeostasis and prevents chronic inflammation. *J. Immunol.* **182**, 3131–3138 (2009).
33. S. A. Koenig Merediz, M. Schmidt, G. J. Hoppe, J. Alfken, D. Meraro, B. Z. Levi, A. Neubauer, B. Wittig, Cloning of an interferon regulatory factor 2 isoform with different regulatory ability. *Nucleic Acids Res.* **28**, 4219–4224 (2000).
34. P. C. Cogswell, R. I. Scheinman, A. S. Baldwin Jr., Promoter of the human NF-κB p50/p105 gene. Regulation by NF-κB subunits and by c-REL. *J. Immunol.* **150**, 2794–2804 (1993).
35. Y. Q. Chen, S. Ghosh, G. Ghosh, A novel DNA recognition mode by the NF-κB p65 homodimer. *Nat. Struct. Biol.* **5**, 67–73 (1998).
36. G. Ghosh, G. van Duyne, S. Ghosh, P. B. Sigler, Structure of NF-κB p50 homodimer bound to a κB site. *Nature* **373**, 303–310 (1995).
37. L. Bintu, N. E. Buchler, H. G. Garcia, U. Gerland, T. Hwa, J. Kondev, R. Phillips, Transcriptional regulation by the numbers: Models. *Curr. Opin. Genet. Dev.* **15**, 116–124 (2005).
38. A. S. Neish, M. A. Read, D. Thanos, R. Pine, T. Maniatis, T. Collins, Endothelial interferon regulatory factor 1 cooperates with NF-κB as a transcriptional activator of vascular cell adhesion molecule 1. *Mol. Cell. Biol.* **15**, 2558–2569 (1995).
39. C. M. Fan, T. Maniatis, Two different virus-inducible elements are required for human β-interferon gene regulation. *EMBO J.* **8**, 101–110 (1989).
40. M. Ptashne, A. Gann, *Genes & Signals* (Cold Spring Harbor Laboratory Press, Cold Spring Harbor, NY, 2002).
41. L. Bintu, N. E. Buchler, H. G. Garcia, U. Gerland, T. Hwa, J. Kondev, T. Kuhlman, R. Phillips, Transcriptional regulation by the numbers: Applications. *Curr. Opin. Genet. Dev.* **15**, 125–135 (2005).
42. C. R. Escalante, E. Nistal-Villan, L. Shen, A. Garcia-Sastre, A. K. Aggarwal, Structure of IRF-3 bound to the PRDIII-I regulatory element of the human interferon-β enhancer. *Mol. Cell* **26**, 703–716 (2007).
43. D. Thanos, T. Maniatis, Virus induction of human IFN β gene expression requires the assembly of an enhanceosome. *Cell* **83**, 1091–1100 (1995).
44. B. S. Parekh, T. Maniatis, Virus infection leads to localized hyperacetylation of histones H3 and H4 at the IFN-β promoter. *Mol. Cell* **3**, 125–129 (1999).
45. D. Panne, T. Maniatis, S. C. Harrison, An atomic model of the interferon-β enhanceosome. *Cell* **129**, 1111–1123 (2007).
46. S. Mathys, T. Schroeder, J. Ellwart, U. H. Koszinowski, M. Messerle, U. Just, Dendritic cells under influence of mouse cytomegalovirus have a physiologic dual role: To initiate and to restrict T cell activation. *J. Infect. Dis.* **187**, 988–999 (2003).
47. L. Wei, M. R. Sandbulte, P. G. Thomas, R. J. Webby, R. Homayouni, L. M. Pfeffer, NFκB negatively regulates interferon-induced gene expression and anti-influenza activity. *J. Biol. Chem.* **281**, 11678–11684 (2006).
48. C. Kunsch, S. M. Ruben, C. A. Rosen, Selection of optimal κB/Rel DNA-binding motifs: Interaction of both subunits of NF-κB with DNA is required for transcriptional activation. *Mol. Cell. Biol.* **12**, 4412–4421 (1992).
49. J. Schreiber, R. G. Jenner, H. L. Murray, G. K. Gerber, D. K. Gifford, R. A. Young, Coordinated binding of NF-κB family members in the response of human cells to lipopolysaccharide. *Proc. Natl. Acad. Sci. U.S.A.* **103**, 5899–5904 (2006).
50. R. Martone, G. Euskirchen, P. Bertone, S. Hartman, T. E. Royce, N. M. Luscombe, J. L. Rinn, F. K. Nelson, P. Miller, M. Gerstein, S. Weissman, M. Snyder, Distribution of NF-κB-binding sites across human chromosome 22. *Proc. Natl. Acad. Sci. U.S.A.* **100**, 12247–12252 (2003).
51. J. Ragoussis, S. Field, I. A. Udalova, Quantitative profiling of protein-DNA binding on microarrays. *Methods Mol. Biol.* **338**, 261–280 (2006).
52. C. L. Warren, N. C. Kratochvil, K. E. Hauschild, S. Foister, M. L. Brezinski, P. B. Dervan, G. N. Phillips Jr., A. Z. Ansari, Defining the sequence-recognition profile of DNA-binding molecules. *Proc. Natl. Acad. Sci. U.S.A.* **103**, 867–872 (2006).
53. S. J. Maerkl, S. R. Quake, A systems approach to measuring the binding energy landscapes of transcription factors. *Science* **315**, 233–237 (2007).
54. G. Badis, M. F. Berger, A. A. Philippakis, S. Talukder, A. R. Gehrke, S. A. Jaeger, E. T. Chan, G. Metzler, A. Vedenko, X. Chen, H. Kuznetsov, C. F. Wang, D. Coburn, D. E. Newburger, Q. Morris, T. R. Hughes, M. L. Bulyk, Diversity and complexity in DNA recognition by transcription factors. *Science* **324**, 1720–1723 (2009).
55. F. E. Chen, D. B. Huang, Y. Q. Chen, G. Ghosh, Crystal structure of p50/p65 heterodimer of transcription factor NF-κB bound to DNA. *Nature* **391**, 410–413 (1998).
56. M. Carey, Y. S. Lin, M. R. Green, M. Ptashne, A mechanism for synergistic activation of a mammalian gene by GAL4 derivatives. *Nature* **345**, 361–364 (1990).
57. A. H. Brivanlou, J. E. Darnell Jr., Signal transduction and the control of gene expression. *Science* **295**, 813–818 (2002).
58. A. E. Mayo, Y. Setty, S. Shavit, A. Zaslaver, U. Alon, Plasticity of the cis-regulatory input function of a gene. *PLoS Biol.* **4**, e45 (2006).
59. N. E. Buchler, U. Gerland, T. Hwa, On schemes of combinatorial transcription logic. *Proc. Natl. Acad. Sci. U.S.A.* **100**, 5136–5141 (2003).
60. F. H. Lam, D. J. Steger, E. K. O'Shea, Chromatin decouples promoter threshold from dynamic range. *Nature* **453**, 246–250 (2008).
61. S. Heinz, C. Benner, N. Spann, E. Bertolino, Y. C. Lin, P. Laslo, J. X. Cheng, C. Murre, H. Singh, C. K. Glass, Simple combinations of lineage-determining transcription factors prime cis-regulatory elements required for macrophage and B cell identities. *Mol. Cell* **38**, 576–589 (2010).
62. A. Hsiao, T. Ideker, J. M. Olefsky, S. Subramaniam, VAMPIRE microarray suite: A web-based platform for the interpretation of gene expression data. *Nucleic Acids Res.* **33**, W627–W632 (2005).
63. K. Cartharius, K. Frech, K. Grote, B. Klocke, M. Haltmeier, A. Klingenhoff, M. Frisch, M. Bayerlein, T. Werner, MatInspector and beyond: Promoter analysis based on transcription factor binding sites. *Bioinformatics* **21**, 2933–2942 (2005).
64. S. L. Werner, D. Barken, A. Hoffmann, Stimulus specificity of gene expression programs determined by temporal control of IKK activity. *Science* **309**, 1857–1861 (2005).
65. S. Basak, H. Kim, J. D. Kearns, V. Tergaonkar, E. O'Dea, S. L. Werner, C. A. Benedict, C. F. Ware, G. Ghosh, I. M. Verma, A. Hoffmann, A fourth IκB protein within the NF-κB signaling module. *Cell* **128**, 369–381 (2007).
66. S. Ogawa, J. Lozach, K. Jepsen, D. Sawka-Verhelle, V. Perissi, R. Sasik, D. W. Rose, R. S. Johnson, M. G. Rosenfeld, C. K. Glass, A nuclear receptor corepressor transcriptional checkpoint controlling activator protein 1-dependent gene networks required for macrophage activation. *Proc. Natl. Acad. Sci. U.S.A.* **101**, 14461–14466 (2004).
67. V. Perissi, A. Aggarwal, C. K. Glass, D. W. Rose, M. G. Rosenfeld, A corepressor/coactivator exchange complex required for transcriptional activation by nuclear receptors and other regulated transcription factors. *Cell* **116**, 511–526 (2004).
68. R. A. Garrick, T. G. Polefka, W. O. Cua, F. P. Chinard, Water permeability of alveolar macrophages. *Am. J. Physiol.* **251**, C524–C528 (1986).
69. J. A. Swanson, M. Lee, P. E. Knapp, Cellular dimensions affecting the nucleocytoplasmic volume ratio. *J. Cell Biol.* **115**, 941–948 (1991).

70. **Acknowledgments:** We thank G. Hardiman and the Biogem core facility and C. Glass for gene expression profiling; C. Benner for his motif search program (Homer); E. Chiang for TLR4-expressing HEK 293T cells; M. Asagiri and T. Huxford (San Diego State University) for the critical review of the manuscript; T. Hwa, V. Nizet, and C. Chang (University of Pennsylvania), as well as members of the laboratory, V. Wang, and V. Veckman for helpful discussions and support. **Funding:** Supported by the Graduate Program in Bioinformatics and Systems Biology and a Department of Defense Breast Cancer Predoctoral Training Fellowship (C.S.C.); the Biomedical Sciences Graduate Program (K.F.); and U.S. NIH grants to A.H. (P50-GM085764 and GM071573), G.G. and A.H. (GM085490), J.P. and A.H. (GM085325), C.A.B. (AI076864 and AI069298), and S.-C.S. (AI057555). **Author contributions:** C.S.C., J.L., K.F., and K.H. performed the experiments; C.S.C. performed computational work; M.C., S.-C.S., S.V., and C.A.B. provided critical reagents and protocols; C.S.C., K.F., and A.H. designed the experiments; C.S.C., K.F., A.H., D.-B.H., J.P., and G.G. analyzed the results; and C.S.C. and A.H. wrote the paper. **Competing interests:** The authors declare that they have no competing interests. **Accession numbers:** The gene expression array data have been deposited in the Gene Expression Omnibus database with the accession number GSE27112.

Submitted 10 September 2010
Accepted 4 February 2011
Final Publication 22 February 2011
10.1126/scisignal.2001501
Citation: C. S. Cheng, K. E. Feldman, J. Lee, S. Verma, D.-B. Huang, K. Huynh, M. Chang, J. V. Ponomarenko, S.-C. Sun, C. A. Benedict, G. Ghosh, A. Hoffmann, The specificity of innate immune responses is enforced by repression of interferon response elements by NF-κB p50. *Sci. Signal.* **4**, ra11 (2011).